Accepted Manuscript

Engineering surface texture and hierarchical morphology of suspension plasma sprayed TiO2 coatings to control wetting behavior and superhydrophobic properties

Navid Sharifi, Fadhel Ben Ettouil, Christian Moreau, Ali Dolatabadi, Martin Pugh

Please cite this article as: Navid Sharifi, Fadhel Ben Ettouil, Christian Moreau, Ali Dolatabadi, Martin Pugh , Engineering surface texture and hierarchical morphology of suspension plasma sprayed TiO2 coatings to control wetting behavior and superhydrophobic properties, *Surface & Coatings Technology* (2017), doi: 10.1016/j.surfcoat.2017.09.034

Title: Engineering Surface Texture and Hierarchical Morphology of Suspension Plasma

Sprayed TiO$_2$ Coatings to Control Wetting Behavior and Superhydrophobic Properties

Navid Sharifi, Fadhel Ben Ettouil, Christian Moreau, Ali Dolatabadi, Martin Pugh[*]

Department of Mechanical, Industrial and Aerospace Engineering

Concordia University

1455 de Maisonneuve Blvd. W, Montreal, Quebec, Canada, H3G 1M8

Abstract:

Beyond its conventional application for developing thermal barrier coatings, suspension

plasma spraying (SPS) has shown promise for new applications focusing on surface textured

coatings including superhydrophobic coatings. Such coatings have a dual-scale hierarchical

morphology or so-called "cauliflower" features on the surface and they demonstrate extreme

water repellence and mobility after treatment for lowering their surface energy. Studying and

determining suitable process parameters to optimize the wetting properties of these coatings is

the focus of this work. Herein, it is demonstrated that by carefully designing and controlling

the process parameters, one can generate relatively fine and uniform dual-scale (hierarchical)

surface textured coatings that after treatment for lowering their surface energy, show

significantly improved water repellence and water mobility with water contact angles as high

as 170° and sliding angles as low as 1.3°. It is also demonstrated that both scale levels of

surface textures (i.e. micron-scale and nanoscale) are essential for having simultaneously

improved water repellence and mobility. Furthermore, it is established that producing finer,

more uniformly distributed and packed surface features lead to more consistent and desirable

wetting properties. The results show the significant influence of pre-deposition surface

---

[*] Corresponding author (martin.pugh@concordia.ca)

roughness, precursor suspension rheology and plasma power on the structure and performance of the developed coatings.

Key words:

Suspension plasma spray (SPS), superhydrophobicity, surface texture, surface morphology, parametric study

1. Introduction

The plasma spraying technique is an efficient and practical method to generate functional coatings for various applications [1–4]. Atmospheric plasma spray (APS) and suspension plasma spray (SPS) have both been largely used for thermal barrier coatings [5], abradable coatings [6] and erosion, corrosion and wear resistant applications [7–9] due to their versatility, deposition rate and scalability. Furthermore, in recent years, new applications have emerged using plasma spraying that are principally focused on generating textured coatings for applications such as superhydrophobic coatings [10,11] and electrochemically active electrodes [12,13]. Due to the novelty of such applications, there is lack of thorough experimental data and published research about them.

Various methods have been used to prepare superhydrophobic coating, including electrodeposition methods [14], vapor deposition [15], lithography [16], laser patterning [17] and sol-gel [18,19]. The vast majority of these works fall into one of two categories: one is using a low surface energy material, the other is using complex methods to tailor the microtexture of the coatings. The former techniques are typically based on polymeric materials that do not demonstrate mechanical durability and the latter techniques are usually very complex and impractical for industrial applications. In the approach presented in this article we take the middle ground using a technique i.e. SPS which is atmospheric and easily applicable onto large surfaces and we demonstrated that the final microtexture of the coatings can be controlled by controlling the process parameters in order to obtain desired coating macrotextures.

In general, a main challenge of working with plasma spray processes is the fact that there are numerous process-related and environment-related parameters that affect the structure, properties and characteristics of the final coating [20,21]. Since these processes are carried out in atmospheric conditions, controlling all influential parameters is required to have adequate

3

control over the resulting characteristics and structures. For the APS process, online diagnosis systems such as DPV and Accuraspray (by Tecnar) [22–24] have been developed making it possible to measure the velocity, temperature and diameter of in-flight particles prior to impact on the substrate. This approach effectively summarizes the effects of process parameter such as plasma power, gas flow and feedstock particle size and provides a comprehensive understanding of the condition of coating formation that greatly facilitates the control and repeatability of the process. However, in the case of the SPS process, since particles are at least an order of magnitude smaller and deposition takes place very close to the plasma jet which is a source of optical noise, online particle diagnostics is challenging and currently under development and investigation. Therefore, to study the effect of process parameters on the suspension plasma spray coatings, it is essential to select a reference set of parameters and then to create a test matrix by changing various parameters one at a time. This allows for investigating the effect of each parameter by isolating the variation of that parameter while constraining the variation of other influential parameters. In the case of parameters that are very difficult to keep constant, such as particle trajectory and substrate temperature, they have been closely monitored to ensure that they remained within a limited range (typically 5% variation).

In recent years, efforts have been made to employ thermal spraying as a relatively fast and efficient surface treatment method for developing coatings with controlled surface wettability. For example Li et al. [25,26] introduced atmospheric plasma sprayed (APS) metallic coatings that demonstrate superhydrophobicity after adsorbing carbon-based components from atmosphere. Guo et al. [27] used vacuum cold spray to deposit a nanostructured coating treated by fluoroalkylsilane that showed highly water-repelling characteristics. Leblanc et al. [28,29] first employed suspension plasma spraying to develop random textured hydrophobic surfaces with reduced drag in interaction with turbulent liquid flow. Chen et al. [30] used flame spraying and a steel mesh as shielding plate to develop cone-like features that improve

4

the wetting behavior of the coating. It is important to note at this point that although some work has been done to study the effect of SPS process parameters [31,32], these investigations has been mainly focused on structural characteristics and properties related to more conventional applications of SPS process such as TBCs.

The main focus of this work is on morphologically textured coatings for roughness-induced superhydrophobic coatings. A thorough parametric study has been carried out to identify the most significant factors that affect the wetting behavior of such coatings and to understand the complex and combined effect of various process parameters as well as morphological features of the coatings. These features form the base of the extreme water repellence and water mobility that these coatings demonstrate. By designing a test matrix of 24 different test conditions and monitoring and controlling the particle jet trajectory and substrate temperature, samples of textured titanium dioxide coatings have been developed. After treating the samples with stearic acid to isolate and diminish the effect of surface chemistry, all samples have been characterized in terms of wettability and the most interesting ones were selected for further visual and morphological characterization. The objective of this work is to quantify and correlate the effect of process parameters and establish a control over surface texture that consequently leads to a control over wetting properties of the coatings.

2. Materials and Methodology:

2.1. Coating Development

All samples were manufactured using the suspension plasma spraying (SPS) technique. For preparation of the feedstock suspension, a commercial submicron-sized titanium dioxide powder with average nominal particle diameter of 500 nm (KS-203A/B, TKB Trading, US) was used. The main objective of this work is to study the macrotextures achieved through SPS process and the influential process parameters to control and design the microtexture to optimize the water repellence and mobility of the coatings. TiO2 has been selected as the coating material because it is an easily available and inexpensive material with minimal safety concerns and reasonable mechanical and chemical stability. Three different suspensions were prepared to study the effect of suspension composition. In two of the suspensions, ethanol was used as the solvent with 10 wt% solid content of TiO_2 for the first and 20 wt% for the second suspension. For both ethanol-based suspensions, polyvinylpyrrolidone (PVP, Alfa Aesar, US) was added (5 wt% of the solid content) as dispersant to ensure the stability of the suspension and to prevent agglomeration and sedimentation during the spraying process. For the third suspension, deionized distilled water was used as the solvent with 10 wt% solid content. For the water-based suspension, polyacrylic acid (5 wt% of the solid content) was used as the dispersing agent. All three mixtures were mixed by magnetic stirring for 5 minutes and then sonicating for 10 minutes with 50 W of power. This routine was repeated once per each 200 ml of suspension. The particle size distribution of each suspension was obtained using a particle size measurement unit (Spraytec, Malvern, UK) and the results are presented in Figure 1 along with a SEM micrograph of the submicron TiO_2 power. Size distribution characteristics of the three suspensions is presented in Table 1.
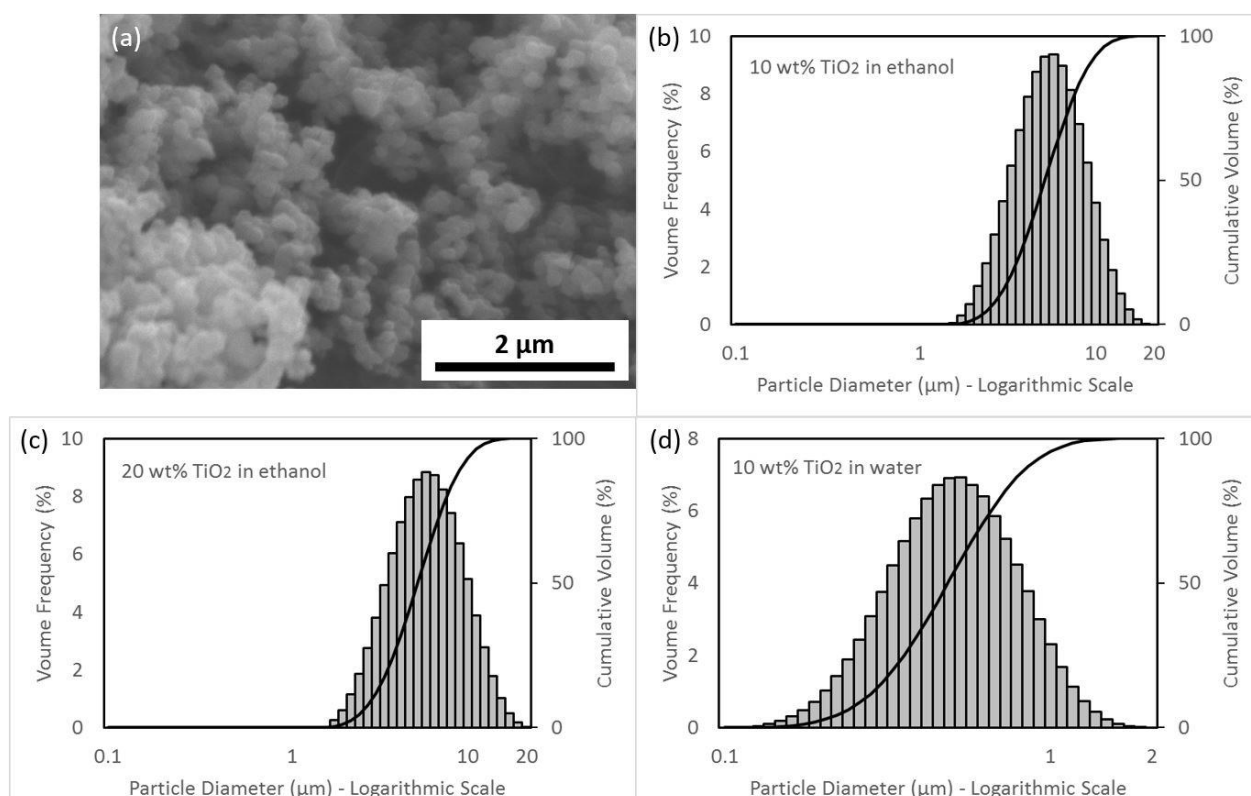
Figure 1. (a) SEM micrograph of the feedstock TiO_2 powder; and (b), (c) and (d) particle size

distribution of the three suspensions used in this study.

Table 1. Size distribution characteristics of the three suspensions used in this work.

Suspension	d10 (μm)	d50 (μm)	d90 (μm)
10 wt% TiO2 in ethanol	2.9	5.1	8.8
20 wt% TiO2 in ethanol	3.0	5.4	9.6
10 wt% TiO2 in water	0.28	0.50	0.86

The coatings were deposited onto flat 304 stainless steel substrates with dimensions of 25 ×

25 × 5 mm³. Prior to the deposition, the substrates were grit-blasted by alumina particles and

then thoroughly cleaned in acetone followed by isopropyl alcohol. To study the effect of

substrate roughness on the morphology and consequently the wettability of the coatings, three

different grit sizes were used, namely 24, 80 and 180 grit that using an air pressure of 354

kPa, which produced a substrate roughness (Ra) of 3.5 μm, 2.5 μm and 1.5 μm, respectively.

These three pre-deposition surface roughness values are labeled C (coarse), M (medium) and

F (fine).

2.2. Test Matrix Design

To deposit the coatings a 3MB plasma torch (Oerlikon Metco, Switzerland) was used. The plasma gas consisted of argon and hydrogen with argon flow rate set on 60 liters per minute and hydrogen flow rate changing to achieve the desired plasma power. The feedstock suspension was stirred during the coating process and was injected radially into the plasma plume as a simple continuous jet with flow rate of 55 grams per minute. Coatings were deposited using 10 consecutive passes of a full spray raster covering the surface of the coupons with a 3 mm overlay distance. To study the effect of various deposition parameters, a test matrix was designed and, overall, eight different combinations of process parameters were used that, combined with three pre-deposition substrate roughness values, produced 24 different samples. The studied parameters include the previously mentioned feedstock suspension compositions, surface roughness prior to deposition, as well as plasma power, plasma torch standoff distance and plasma nozzle diameter. Plasma power was modified by changing the arc current and the amount of hydrogen gas which increases the voltage of the plasma. It is important to note that the reported plasma power here is the input electrical power of the plasma. The thermal efficiency of the process is not measure here but studies on similar working condition typically reported a thermal efficiency of 55-60% [33]. A detailed list of the parameters used to design this test matrix and the corresponding abbreviations are presented in Table 2. The test matrix is detailed in Table 3.

Table 2. Values of variable process parameters and the corresponding abbreviations used in this study.

Variable Parameter	Levels	Abbreviations
Grit-blast	Coarse, Medium, Fine	C, M, F
Suspension solvent	Ethanol, Water	E, W
TiO_2 weight percent	10, 20 (wt%)	10%, 20%
Plasma power	25, 36 kW	LP, HP
Standoff distance	3, 5 (cm)	LSD, HSD
Plasma torch nozzle diameter	5, 8 (mm)	SND, LND

Table 3. Test matrix parameters used in this study.

Condition	Solvent	TiO$_2$ (wt%)	Grit-blast	Plasma power (kW)	Standoff distance (mm)	Plasma nozzle (mm)
10-E-LP	E	10	C, M, F	25	50	8
10-E-HP	E	10	C, M, F	36	50	8
10-E-LSD	E	10	C, M, F	25	30	8
10-E-SND	E	10	C, M, F	25	50	5
10-W-LP	W	10	C, M, F	25	50	8
10-W-HP	W	10	C, M, F	36	50	8
20-E-LP	E	20	C, M, F	25	50	8
20-E-HP	E	20	C, M, F	36	50	8

During the deposition process, the Accuraspray system (Tecnar, Canada) was used to monitor the trajectory of the particle jet to ensure the proper penetration of the particle jet into the plasma plume. Accuraspray is an optical diagnosis unit capable of measuring velocity and temperature of the cloud of particles. The temperature measurements by the Accuraspray system for SPS process are accompanied by optical noise from plasma due to short spray distance and therefore are not reported in the study. However, the sensor still receives signals from particles that are passing in front of it. Accuraspray software analyzes these signals and identifies the center of the particle jet which slightly deviates from the center of the plasma jet due to axial injection of the particles. In this work, it was confirmed using Accuraspray that the deviation of the center of the particle jet from the center of the plasma plume remained within a range of 6% of the spray distance. This was achieved by slightly adjusting the angle of injection of suspension and without changing plasma gas flow rate. Additionally, to further increase the repeatability of the results and consistency of the comparative study, an infrared camera (A310, FLIR, US) was used to monitor the temperature of the substrate during the deposition process. Two air amplifiers (devices that direct a high volume and high velocity flow of air toward a target) were used during all tests to cool down the substrate and maintain the surface temperature below 600°C in all conditions.

In the suspension injection system, a mass flow meter was used to ensure the constant and steady feeding of the suspension feedstock into the plasma and the density of the suspension was constantly monitored online using a Coriolis flow meter to ensure the quality and characteristics of the suspension were constant during the coating process.

2.3. Surface Treatment

After coating, samples were sonicated in deionized distilled water to discard loose solid particles. Afterwards, the samples were thoroughly cleaned in acetone followed by isopropyl alcohol. To make sure the surface of the samples were free of organic contamination from the acetone or isopropyl alcohol, the samples were placed in boiling deionized distilled water as proposed by Gentlemen et al. [34]. In order to reduce the surface energy and also isolate and study the effect of surface roughness on the wetting behavior of the coatings, all samples were dipped into a 0.5 wt% solution of stearic acid in 1-propanol and then dried using compressed dry air [11]. A flat sample treated with stearic acid using the same method yields a contact angle of 97° and sliding does not occur on such surface.

2.4. Characterization

To assess the wettability of the different coatings, multiple wetting parameters were measured and compared for all 24 coatings. First of these wetting parameters is static contact angle (CA) which was measured by imaging a 5 μl droplet of high purity deionized distilled water and analyzing the image using a plugin in the image analysis software ImageJ, developed by Stadler et. al. [35,36]. The second wetting parameter is sliding angle which was measured by placing a droplet of the same size on the surface of the sample, then tilting the sample using a goniometer until the droplet started to move on the surface. The angle at which the droplet starts to move is taken the sliding angle.

The coatings were grouped based on their wetting behavior with respect to the following criteria: for static contact angle, a larger value is better with contact angles higher than

150°considered satisfactory. For sliding angle, a smaller value is better with values smaller than 10° typically considered ideal. Based on these criteria, a third of the samples with the most desirable properties were selected for further analysis as well as a few samples with less desirable wettability which were further analyzed to understand the morphological characteristics that lead to poor performance.

In the next stage of characterization, the top surfaces of the selected samples were examined using a scanning electron microscope (SEM) [S-3400, Hitachi, Japan]. Micrographs were obtained from the top of all samples at identical magnifications to be able to compare the size, shape and distribution of morphological features and their effect on wettability of the coatings and consequently, the effect of various deposition parameters on the wetting behavior through the variation in corresponding surface morphology. To further study the effect of pre-deposition substrate surface roughness, some selected samples were cut and polished to analyze their cross-sections. These samples were cleaned, then molded in a cold mount resin, ground and polished per standard metallography procedures to prepare cross-section views. These samples were studied using SEM and micrographs of the coatings and coating/substrate interface were taken.

To further investigate roughness features and properties of the coating surfaces, a confocal laser microscope [LEXT OLS4000, Olympus, Japan] was employed. Using the microscope, three 3D maps of the surface of the coatings in 12mm × 2mm areas were obtained in three different spots on the same sample. Each image consists of 96 (24 by 4) single images, digitally stitched together to generate the three-dimensional map of the area which is large enough to be considered an average representation of the surface. Using this image and analytical software, all surface roughness parameters per ISO 25178 were calculated and studied for potential correlation with the wetting behavior of the different coatings. Various surface roughness parameters are presented as some studies [19,37] have shown that topographical characteristics of a surface cannot be accurately represented using only one

11

surface roughness parameters with one work [38] relating root mean square height of the surface (S_q) to wetting behavior, and others [39] claiming correlation between wettability to skewness (S_{sk}) and kurtosis (S_{ku}) of the surface. Additionally, the surface ratio of the coating surface defined as the ratio of real surface area to the projected surface area was measured and studied. It is noteworthy that since the confocal laser microscopy technique is a line of sight technique, it typically underestimates the value of real surface area but neglecting additional surface area hidden from line of sight. However, since in this work we study the wetting properties of the surface which is affected by interaction of water droplet and the surface, it is expected that the surface ratio, although not a perfect representative but to be an indicator of wetting behavior of the surface. All the aforementioned surface parameters were investigated for a potential correlation with wetting behavior of the coatings. For this purpose the coefficient of correlation was calculated for each surface roughness parameters in respect to the contact angle and sliding angle of the coatings. The parameters with highest relative correlations were selected and used to plot the graphs shown combined effect of surface parameters on wettability of the coatings.

3. Results and Discussion:

In Figure 1, the particle size distribution of the three feedstock suspensions is presented. Noting that the average particle size distribution of the TiO_2 particles is 500 nm, in the water-based suspension the particles are almost completely dispersed with a nearly perfect Gaussian distribution. However, in the case of both ethanol-based suspensions, a different size range of distribution is observed. This shows that majority of particles are either single or formed small aggregates in the water-based suspension, while a considerable portion of the particles in the ethanol-based suspension formed aggregates with diameters ranging between a few micrometers to a few tens of micrometers. It is noteworthy that the particle size distribution of the two ethanol-based suspensions (10 wt% and 20 wt%) is very similar which shows that in this range, the concentration of TiO_2 particles does not considerably affect the size distribution.

3.1. Wettability

Table 4 presents a summary of wetting tests in terms of water contact angle (WCA), sliding angle (SA). Additionally, the surface roughness measurements results including arithmetical mean height of the surface (S_a), maximum height of the surface (S_z), root mean square height of the surface (S_q), Skewness of height distribution (S_{sk}), and kurtosis of height distribution (S_{ku}) are presented. From this table, it is observed that all samples have relatively high water contact angle (WCA) values with the majority of samples having a contact angle higher than 150°. However, as previously mentioned, high water contact angles alone cannot guarantee the superhydrophobic behavior of a surface as it only represents the water repellence. To understand the water mobility of a surface, which plays an equally important role in superhydrophobicity, it is necessary to consider the sliding angle values of the surfaces. While some of the samples show sliding angles higher than 10° which is considered the threshold of superhydrophobicity in this article, some other samples show promise with sliding angle

values smaller than 10° and in some cases even smaller than 5°. These coatings are the most interesting ones in terms of wettability and surface texture and are examined further. Additionally, the effect of process parameters on wetting behavior of the surface is further analyzed in this article by considering their effect on sliding angle.

Table 4. Coating wetting characteristics including: water contact angle (WCA) and sliding angle (SA), and surface roughness measurements including: arithmetical mean height of the surface (S_a), maximum height of the surface (S_z), root mean square height of the surface (S_q), skewness of height distribution (S_{sk}), kurtosis of height distribution (S_{ku}). [mean±SEM]

Condition	Grit-blasting	WCA (°)	SA (°)	S_a (µm)	S_z (µm)	S_q (µm)	S_{sk}	S_{ku}
10-E-LP	C	165±1	11.7±1.7	7.0±0.1	81.0±2.6	8.7±0.2	-0.164 ±0.012	2.9±0.1
	M	162±1	10.3±1.2	5.8±0.1	74.3±2.4	7.3±0.1	-0.479 ±0.049	3.4±0.1
	F	165±1	10.1±0.7	5.7±0.1	62.5±2.3	7.1±0.2	-0.233 ±0.018	3.0±0.1
10-E-HP	C	166±1	4.1±0.5	10.4±0.1	108.8±6.8	13.0±0.2	0.497 ±0.015	3.2±0.1
	M	165±1	3.7±3.7	9.1±0.1	95.8±2.1	11.6±0.2	0.229 ±0.021	3.1±0.1
	F	168±1	1.3±0.3	8.3±0.1	82.1±2.9	10.4±0.1	0.515 ±0.008	3.0±0.1
10-E-LSD	C	164±1	16.3±1.1	6.7±0.2	89.5±2.7	10.2±0.2	0.244 ±0.024	3.1±0.1
	M	155±1	13.3±1.0	5.8±0.2	71.3±4.9	7.3±0.2	0.407 ±0.042	3.2±0.1
	F	165±1	9.8±1.0	5.5±0.1	66.1±2.2	7.0±0.1	0.274 ±0.054	3.3±0.1
10-E-SND	C	165±1	6.2±0.5	10.1±0.1	100.9±1.5	12.6±0.1	0.246 ±0.016	2.9±0.1
	M	159±1	7.2±0.5	7.7±0.1	102.1±15.1	9.6±0.2	0.288 ±0.033	3.6±0.5
	F	163±1	5.3±0.7	8.7±0.2	88.8±2.7	10.8±0.3	0.327 ±0.017	3.0±0.1
10-W-LP	C	137±8	>20	5.1±0.1	71.0±3.3	6.6±0.1	0.566 ±0.041	3.9±0.2
	M	140±5	>20	4.1±0.1	58.7±1.6	5.3±0.1	0.520 ±0.045	4.2±0.2
	F	142±3	>20	3.3±0.1	51.7±3.4	4.2±0.1	0.227 ±0.045	4.0±0.2
10-W-HP	C	154±1	14.2±1.8	6.2±0.1	79.2±1.5	8.5±0.1	0.559 ±0.022	3.8±0.1
	M	152±1	11.1±2.2	4.7±0.2	73.5±3.6	6.2±0.3	0.543 ±0.091	4.5±0.1
	F	159±1	8.4±1.3	5.6±0.2	67.9±3.1	7.4±0.3	0.802 ±0.039	4.0±0.1
20-E-LP	C	165±1	3.8±1.7	8.3±0.1	97.4±7.5	10.2±0.1	0.247 ±0.054	3.0±0.2
	M	169±1	3.4±1.9	8.8±0.2	87.7±2.5	8.4±0.2	0.247 ±0.009	2.8±0.1

	F	170±1	1.4±0.3	8.5±0.1	89.4±3.7	7.8±0.3	0.305 ±0.019	3.0±0.1
	C	157±1	7.1±0.9	10.4±0.3	99.2±2.5	12.9±0.4	0.632 ±0.006	3.0±0.1
20-E-HP	**M**	155±1	6.3±0.4	9.3±0.2	91.0±4.6	11.6±0.3	0.790 ±0.009	3.2±0.1
	F	160±1	4.0±0.5	9.9±0.2	88.3±1.0	12.3±0.2	0.795 ±0.007	3.1±0.1

Since the surface chemistry is the same for all coatings, the different wetting behaviors are linked to the different coating micro-textures. It is important to study the surfaces with different wetting characteristic to better understand the features and morphological properties that result in such wetting behavior. In Figure 2, six of the coatings with distinguishably different wetting behaviors are selected and the SEM micrographs of their surface morphology at two magnifications are presented.

3.2. Surface Morphologies

A simple side by side visual comparison of micrographs presented in Figure 2, reveals that the morphology of the coatings varies significantly depending on the deposition conditions. In general, using water-based suspension as feedstock [Figure 1-(b)] results in a rather mono-scale roughness and the so-called "cauliflower features" with hierarchical morphology are absent. In coatings developed using the water-based suspension (Figure 2 (a) and (b)) the primary surface texture features or so-called cauliflower-like features are not fully formed and clearly distinguishable. In fact, these coatings have only a single scale of roughness instead of the desired hierarchical texture. On the other hand, in ethanol-based coatings, surface microtexture features with two distinguished size-scales are observed. The smaller scale features are similar to those observed in the water-based process, while the larger scale features (cauliflowers) are unique to the ethanol based coatings. This is partly due to the previously mentioned particle size distribution of the water-based suspension which consists of many fully dispersed solid particles with fewer and smaller aggregates as well as rheological properties of water in comparison to ethanol. The combined effect of suspension

characteristics affects the atomization of suspension in the cross-flow interaction with the plasma which significantly influences the coating morphology. Based on the results, there is a considerable difference in the microtexture of the coatings deposited using water-based and ethanol-based suspensions. This difference can be the result of combination of factors including dispersion of solid particles in the suspension, different in atomization and the relatively large specific heat capacity and latent heat of vaporization of water in comparison to ethanol. This results in solid particles to be heated less in case of the water-based suspension that produces more unmolten particles. This can be another reason for the coatings deposited through water-based suspension to lack the desired hierarchical texture.
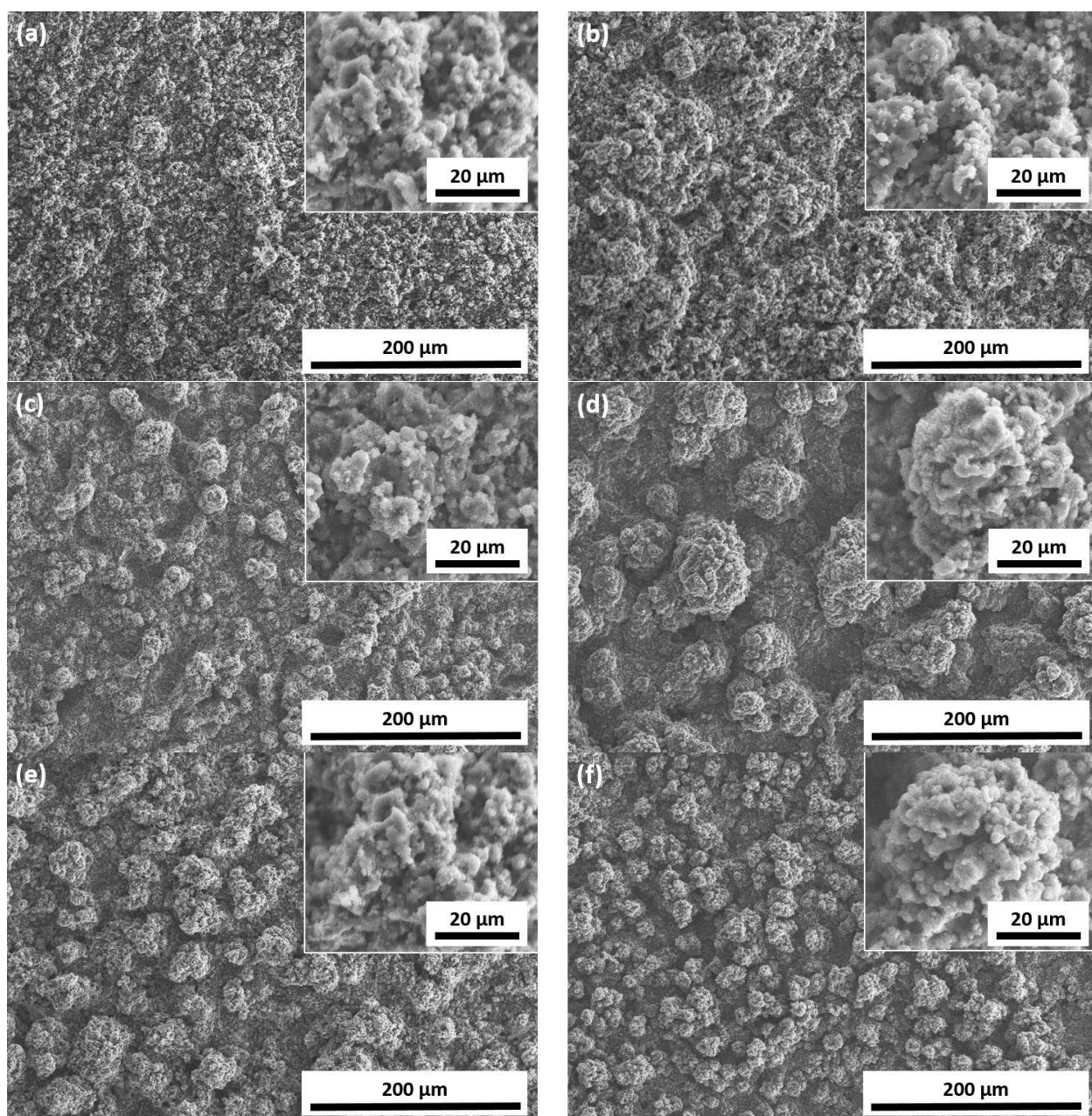
Figure 2. SEM micrographs of selected samples deposited though six spraying conditions and representing various surface textures and wetting behaviors. Samples are sorted in order of increasing water repellency and mobility: (a) condition 10-W-LP-M, (b) condition 10-W-HP-M, (c) condition 10-E-LP-M, (d) condition 20-E-HP-M, (e) condition 20-E-LP-M, (f) condition 10-E-HP-F.

As previously mentioned, the SEM micrographs in Figure 2 are sorted in order of increasing water repellency and mobility which corresponds to increasing superhydrophobicity and thus desirability. Close investigation of the micrographs reveal that the improvement in water

repellence and mobility can be attributed to two morphological characteristics in these coatings. The first characteristic is the presence of so-called cauliflower-like features on the surface. As seen in the larger magnification inserts in Figure 2, at the secondary submicron scale of roughness, all coatings have similar features. It is known that this secondary roughness in a hierarchical morphology has an important role to stabilize the water-solid interface and improve the superhydrophobicity [40]. However, as seen in Figure 2 (a) and (b), this submicron roughness alone cannot generate high water repellence and mobility. In fact, the formation and presence of primary roughness features which provides entrapment of air between the solid and water at the interface is necessary to achieve extreme water repellence and mobility. This primary texture is believed to form because of a phenomenon known as the shadow effect in suspension plasma spraying [41,42]. This effect comes into play when initial deposition of particles on the surface creates some bumps that affects the incoming particles' trajectory, causing them to attach to the surface of these bumps and preventing them from attaching to the surrounding regions. This mechanism is the main cause of formation of cauliflower-like features.

The second noteworthy characteristic of the surface texture is uniformity and refinement of the cauliflower-like features. In Figure 2 (c) and (d), it is observed that, although these two coatings demonstrate some of the hierarchical features, in the first coating texture, these features are not fully developed and packed while in the second coating texture, the hierarchical features are relatively large and distant. In both cases, when a water droplet is sliding on these surface, if at some points the features are not fully developed or there is a relatively large gap between them, the droplet gets trapped at those points which causes an increase in sliding angle and reduction of mobility. Finally, looking at Figure 2 (e) and (f) which are the surface textures that provide the highest mobility, fully developed and packed hierarchical features ultimately result in a surface on which a water droplet easily slides and

has extremely high mobility. This is particularly true for the last surface texture which has finer and more uniform features and can provide a sliding angle as low as 1.3°.

3.3. Effect of grit-blasting

The effect of grit-blasting with three different grit sizes is shown in Figure 3. Accordingly, by moving from coarse to fine grit size, the sliding angle generally decreases. This effect is observed for seven of the original eight deposition conditions. However, for the case of the water-based suspension at low power, the sliding angle is so large that it is practically impossible to measure the sliding angle consistently and therefore the effect of grit-blasting cannot be correctly determined. In Figure 4, SEM micrographs of the cross-section of coatings for 10 wt% TiO_2 ethanol-based suspension deposited at high power respectively on coarse (C), medium (M) and fine (F) grit-blasted coupons are shown. These three coatings have been deposited with the same spray conditions with the only difference being in grit-blasting of the substrates before deposition. By comparing these three SEM micrographs and according to Figure 3, it can be concluded that it is the combination of deposition condition and not only the surface grit blasting that determines if hierarchical morphology is developed in the coatings or not. However, for coatings sprayed in other spray conditions, finer grit-blasting results in finer and more uniform surface features that improves both water repellence and mobility and thus is more desirable.

It needs to be noted that investigating the adhesion of the coating to the substrate using conventional bond strength measurement techniques is not practically possible to the relatively low thickness and high porosity and surface roughness of the coatings. For practical applications such as icing and water erosion the mechanical durability of these coating are to be thoroughly investigated in the future, however, we can report that we have not observed any sign of failure or delamination in the coatings during the process of investigation.
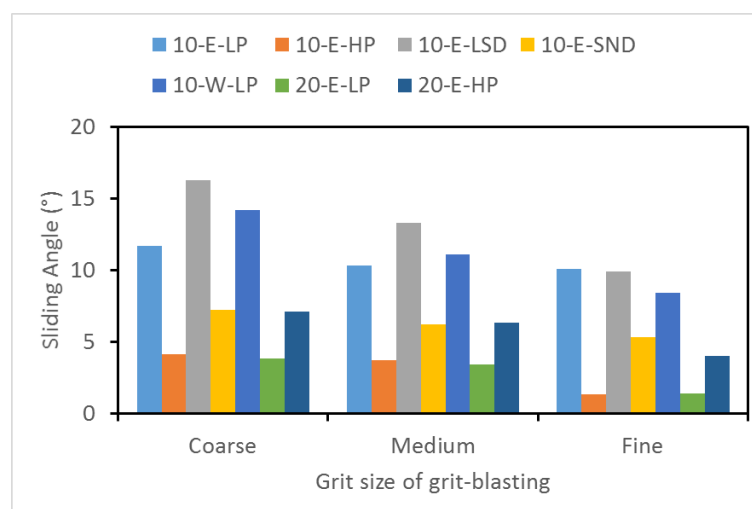
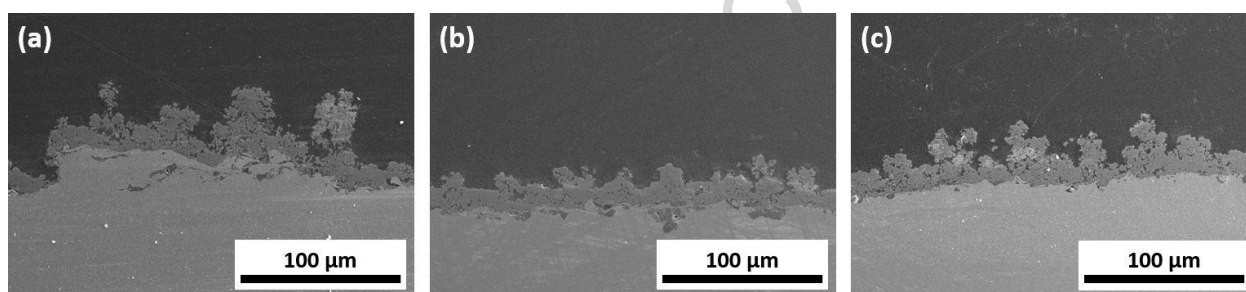Figure 3. Effect of grit size on sliding angle of the coatings.

Figure 4. SEM micrographs of the cross-section of the coatings deposited at the same process condition with different substrate roughness: (a) 10-E-HP, coarse, (b) 10-E-HP, medium, and (c) 10-E-HP, fine grit-blast.

3.4. Effect of suspension solid content and plasma power

The effect of suspension solid content on sliding angle of the coatings is shown in Figure 5. In the case of the low power condition, all three coatings show lower sliding angles while increasing the suspension solid content. On the contrary, for high power conditions, increasing the suspension solid content has the reverse effect, reducing the water mobility of the coatings. This apparent contradiction, can be explained by considering the interaction of the suspension feedstock with the plasma plume. It is speculated that, at low power, increasing the solid content of the suspension does not greatly affect the deposition rate as the plasma does not have sufficient power to considerably change the amount of fully molten and

20

deposited particles. In this case, more semi-molten particles cause formation of rougher and more irregular features on the surface that, in turn, improve the mobility of the surface. On the other hand, at high power, the plasma has sufficient power to melt the additional TiO_2 particles and therefore the deposition rate increases. This causes the 20 wt% suspension coating to grow faster which results in larger and more distant morphological features. This is further supported by noticing the relatively larger size of features in Figure 2 (d) and by relatively larger thickness of the coating resulted from the 20 wt% suspension deposited in high power condition.
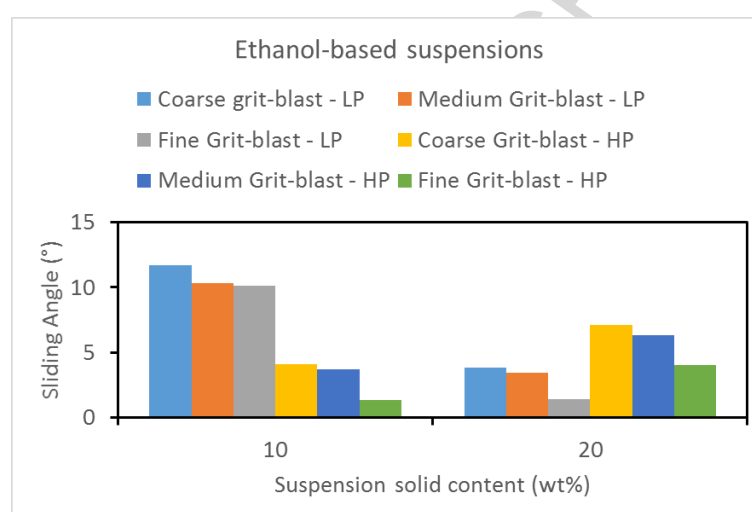

Figure 5. Effect of suspension solid content on sliding angle of the coatings.

To compare the deposition rates, the thickness of the coatings deposited using 10 wt% and 20 wt% suspensions for the two power levels 25 kW and 36 kW were measured and the result is reported in Table 5. As it can be seen the deposition rate increases more in the case of 25 kW compare to 36 kW which agrees with the discussion made earlier.

Table 5. The deposition rate for different powers and suspension solid contents.

Suspension solid content	Coating deposition rate	
	25 kW plasma power	36 kW plasma power
10 wt%	1.8	2.1
20 wt%	3.5	3.6

Figure 6 (a) and (b) show the effect of plasma power on the sliding angle for the 10 wt% and 20 wt% ethanol-based suspensions respectively. For the 10 wt% suspension, an increase of the plasma power induces a significant decrease of the sliding angle. The same effect was observed for the water-based suspension since, at low power, these coatings show relatively high (>20°) sliding angles whereas, at high power, these coatings have noticeably lower sliding angle values. However, this effect is reversed for 20 wt% ethanol-based suspension where increasing the plasma power increases the sliding angle. The reason for this behavior as previously mentioned, is believed to be related to a significant increase in deposition rate in the case of the high power deposition of the 20 wt% suspension that results in the formation of relatively large texture features which decrease mobility.
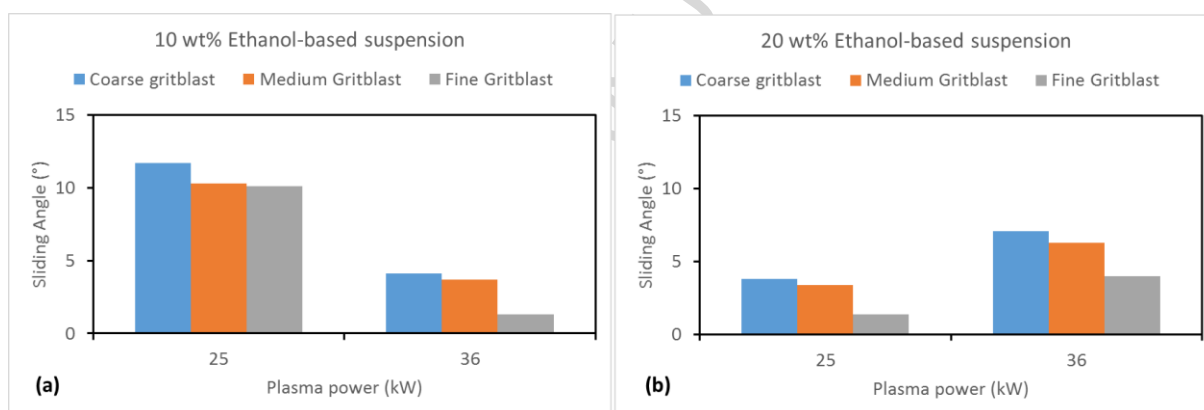

Figure 6. Effect of plasma power on sliding angle of the coatings.

3.5. Effect of standoff distance

The effect of changing standoff distance on sliding angle is presented in Figure 7. It is observed that generally the sliding angle increases when the standoff distance is reduced. In SPS, the standoff distance is relatively small, compared to other thermal spray processes, and the deposition is greatly affected by the turbulent plasma gas flow pattern close to the substrate. In this case, a standoff distance of 3 cm changes the flow pattern significantly and affects the deposition mechanism and formation of hierarchical features preventing the desired surface texture to form correctly and causing the surface mobility to decrease.
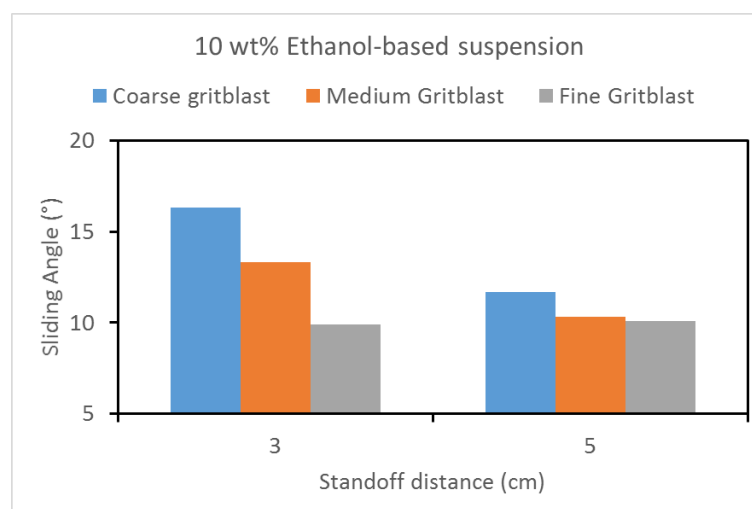
Figure 7. Effect of standoff distance on sliding angle of the coatings.

The SPS is complex process that has many influential parameters, and it is difficult to speculate about all observed phenomena. This is particularly true about the influence of spray distance as it is difficult to study the particles' behavior in flight. However, in all mentioned cases, it is observed that sliding angle is relatively large which means that in these coatings the desired features are not fully developed. It is known that the surface roughness has a major role in creating the shadow effect which is the main mechanism responsible for formation of microtexture features. We can speculate that this effect is more pronounces for 3 cm spray distance because surface roughness influences the flow close to the surface and affects the deposition of the particles. However, as mentioned previously since none of these coatings are among the best performing coatings, we have focused more on more interesting deposition condition.

It is important to note at this point that it has been reported in the literature that [32] spray distance is the only SPS process parameter that influences the phase distribution and ratio of anatase to rutile in SPS TiO_2 coatings. Additionally, typically rutile is the more likely phase to form during plasma spraying of TiO_2 [43] due to high cooling rate. However, in this study, as the coatings are all treated similarly in the stearic acid solution, it is not expected that difference in intrinsic wetting properties of rutile and anatase affect the wetting properties of

23

the coatings. In other words, it is the surface microtexture and not the phase distribution that is the determining factor in wetting behavior of coating developed in this study.

3.6. Effect of plasma gas velocity

Figure 8 shows the effect of changing the diameter of the plasma nozzle on the sliding angle of the coatings. By decreasing the diameter of the plasma nozzle and keeping all other parameters the same, the velocity of the plasma gas increases which in turn increases the velocity of the particles and decreases the time that particles travel in the plasma plume. According to the results, increasing the plasma gas velocity through using a smaller plasma nozzle has a positive effect on mobility of the water on the coatings.
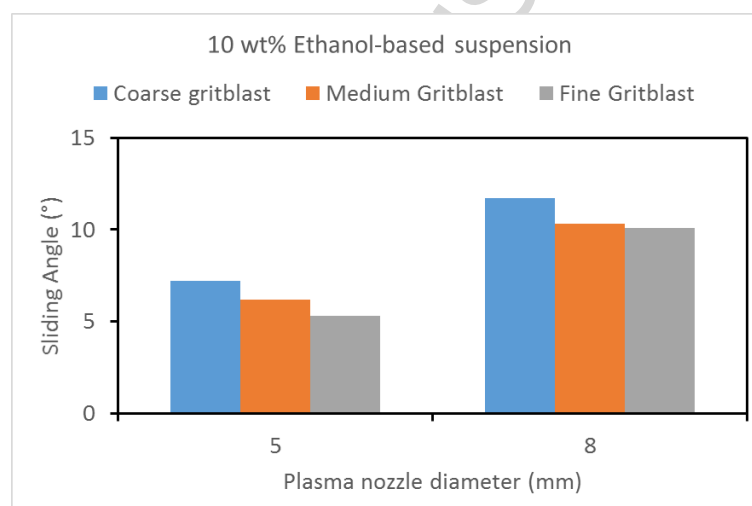

Figure 8.Effect of plasma nozzle diameter (and consequently plasma gas velocity) on the sliding angle of the coatings.

3.7. Topography

In Table 4, multiple surface roughness parameters of the coatings are presented. The first three parameters, arithmetical mean height of the surface (S_a), maximum height of the surface (S_z), root mean square height of the surface (S_q), are all amplitude parameters that relate to the general roughness of a surface. More than one of these parameters is required to represent the actual characteristics of a surface. While all of these parameters show a coefficient of

correlation smaller than 0.9 in regards to water contact angle or sliding angle of the samples, they collectively demonstrate an appropriate measure of the roughness of the coatings and it can be concluded that a minimum amplitude of roughness is necessary for these coatings to show reasonable degree of superhydrophobicity.

Skewness (S_{sk}) and kurtosis of height distribution (S_{ku}) are also shown in Table 4. Skewness and kurtosis provide additional information about the shape and type of the roughness on the surface of the coatings. A schematic in Figure 9 shows the type of surface features and the corresponding skewness and kurtosis values.
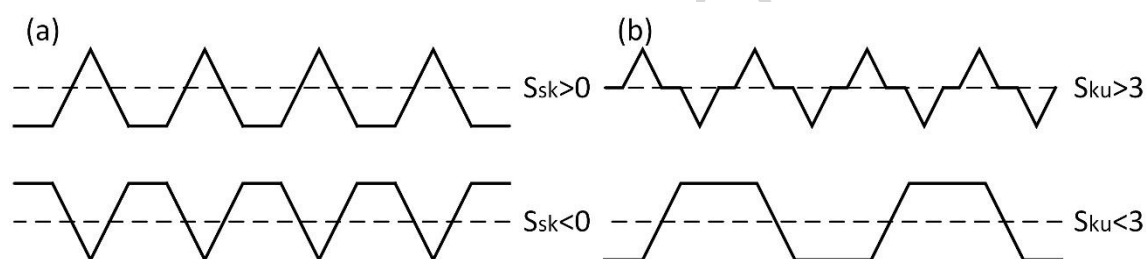

Figure 9. Schematic showing the types of surfaces and corresponding skewness and kurtosis values: (a) positive and negative skewness; (b) kurtosis larger and smaller than 3.

According to Table 4, the majority of the developed coatings have positive skewness values. In the case of the few negative skewness values, the coatings do not show promising water mobility. This can be explained by the fact that a negatively skewed surface does not allow the formation of large air pockets in the water-solid interface and also results in more solid/liquid interfacial area which reduces the mobility of the surface. In terms of kurtosis, the majority of the coatings have a kurtosis close to 3 which represents their distribution of the peaks and valleys. The coatings that have a relatively large divergence from the normal distribution and their kurtosis value is far from 3 typically do not show significant improvement in water mobility.

A study of correlation coefficient between various surface topographical parameters and surface wettability revealed that the ratio of actual surface area to projected surface area

(surface ratio) has the highest correlation coefficient in respect to sliding angle with a value of -0.81 followed by arithmetic mean height with a value of -0.75. Among non-height surface roughness parameters, kurtosis shows the largest correlation with a correlation coefficient of 0.63. Figure 10 shows a graph, depicting the variation of the sliding angle of the coatings against the two factors with largest correlation coefficients i.e. the surface ratio and the arithmetic mean height (S_a) of the samples. A second order polynomial is fitted on the data with a coefficient of determination (R^2) of 0.75 and 0.68 respectively.
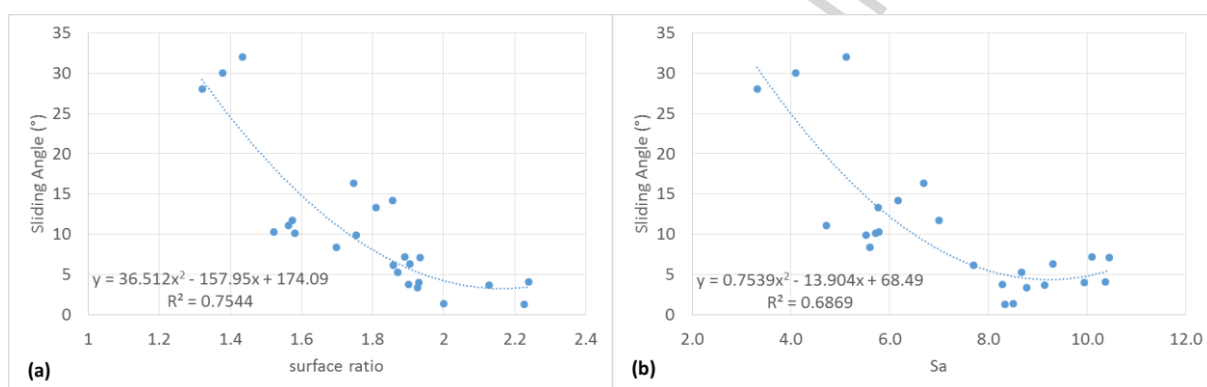

Figure 10. Graphs showing the correlation between the sliding angle of the coatings and (a) surface ratio; and (b) arithmetic mean height (R_a) roughness.

In Figure 11, two graphs are constructed by plotting the arithmetical mean height of the surface and kurtosis of the coatings surfaces versus the surface ratio of the coatings and the sliding angle value obtained for these coatings is represented by the size of the circles. In these graphs, smaller circles which show coatings with higher water mobility are desirable. As previously mentioned, there is not a single surface roughness parameter that determines or predicts the wetting behavior of a surface. However, looking at a combination of the surface parameters that show the best correlation with the desired wetting behavior (i.e. lower sliding angle and higher mobility), it is possible to identify surface characteristics that seem to indicate improvement in surface wetting behavior. As seen in Figure 11(a) and (b), there are areas (shown by dotted red ovals) in which most coatings with better water mobility are located. In both cases, it is clear from the graphs that larger surface ratios are favorable to

26

achieve higher superhydrophobicity. Furthermore, it can be concluded that a minimum height in terms of S_a is required to achieve the best result, whereas kurtosis values that deviate too much from normal distribution (i.e. $S_{ku}=3$ which corresponds to similar number and height of valleys and peaks in the surface topography) are not desirable.
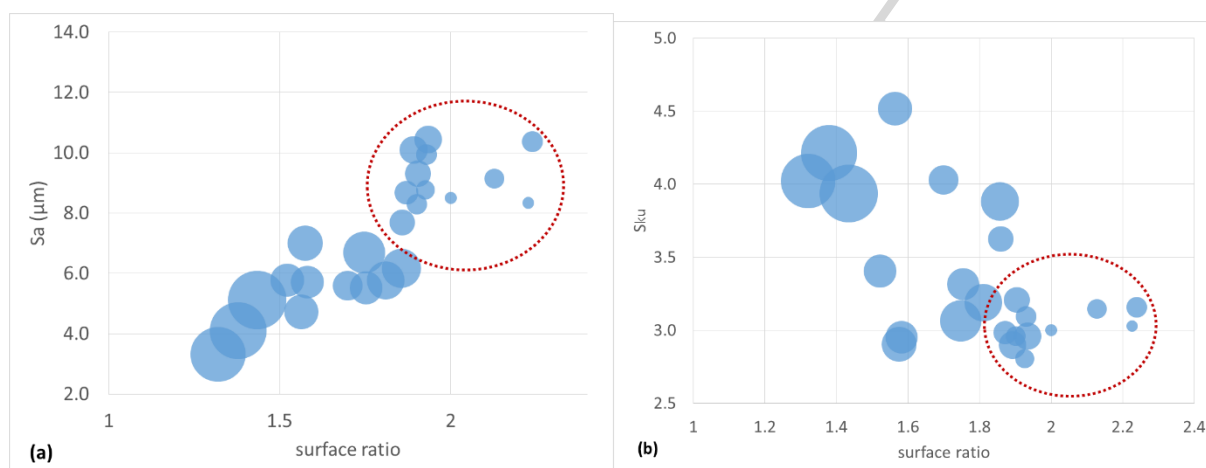

Figure 11. (a) Arithmetic mean height of the surface (S_a) plotted against the surface ratio and (b) kurtosis (S_{ku}) of the surface plotted against the surface ratio for all the coatings. The size of the circles is proportional to the value of the sliding angle of each coating, thus the smaller the circle the better the mobility of the coating.

Figure 12 schematically demonstrates some of the major conclusions of this study. As shown, finer grit-blasting of the surface prior to deposition results in more refined and more packed 'cauliflower-like' surface features. Such surface microtexture leads to improved water mobility i.e. small sliding angles. It is important to note that as previously mentioned both primary and secondary roughness features are essential for achieving desired wetting properties in the coatings.
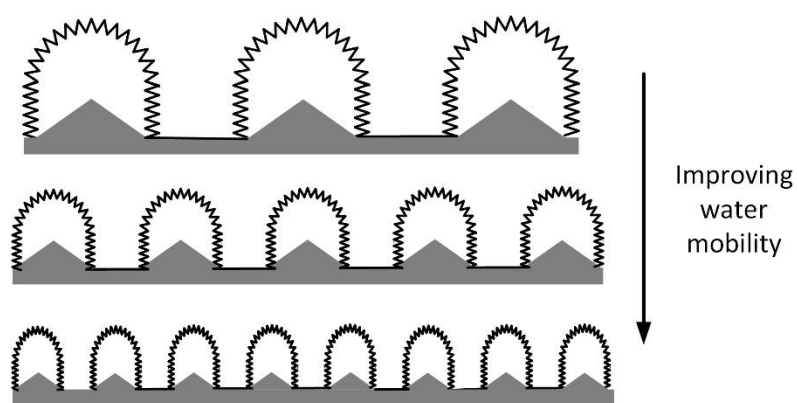
27

Figure 12. A schematic based on findings of this work that demonstrates how refinement of surface texture leads to improvement in water mobility of the surface.

4. Summary and Conclusion

The effect of SPS process parameters including substrate roughness, suspension composition and solid content, plasma power, standoff distance and plasma gas velocity on wetting behavior and surface texture of TiO_2 coatings was investigated. It is shown that plasma power, suspension composition and solid content and plasma gas velocity are the most influential parameters while grit-blasting size has a moderate effect. Plasma power improves the surface water mobility for both 10 wt% ethanol-based and water-based suspension coatings, whilst it has an opposite effect on 20 wt% ethanol-based suspension coatings. This is believed to be related to increased deposition efficiency at higher power and higher suspension solid content which results in larger surface features. Water-based suspension is not promising as it generates coatings without the needed hierarchical features. These features are shown to be critical to achieve both high surface water repellence and mobility. In addition to the presence of hierarchical features, the finer and more uniform these features are, the better the wetting behavior of the coatings, making some of them extremely superhydrophobic. Fine grit size during surface preparation has shown to be influential in generating finer and more packed surface textures. The two best coatings in this study in terms of superhydrophobic performance were achieved using ethanol-based TiO_2 suspension as feedstock deposited onto substrates grit-blasted with the finest grit size and with a plasma gun standoff distance of 50 mm. The best 10 wt% solid content suspension was deposited in high power condition (36 kW) while the best 20 wt% suspension was deposited in low power condition (25 kW). Both these coatings showed extremely high water repellence and mobility manifested by contact angles larger than 165° and sliding angles smaller than 1.5°, respectively. The best coatings developed in this work are comparable to the best results reported in the literature [40,44] in terms of wetting properties.

Acknowledgement

References

[1]   R.C. Tucker, P.S.T. Inc, Thermal Spray Coatings, Handb. Surf. Eng. (1993) 1446–
        1471. doi:10.1007/s11548-011-0634-9.

[2]   J.R. Davis, Thermal Spray Technology Edited by, Technology. (2004).

[3]   L. Pawlowski, The Science and Engineering of Thermal Spray Coatings, 2008.
        doi:10.1002/9780470754085.

[4]   P.L. Fauchais, J.V.R. Heberlein, M.I. Boulos, Thermal Spray Fundamentals, 2014.
        doi:10.1007/978-0-387-68991-3.

[5]   W. Beele, G. Marijnissen, A. van Lieshout, The evolution of thermal barrier coatings
        — status and upcoming solutions for today's key issues, Surf. Coatings Technol. 120
        (1999) 61–67. doi:10.1016/S0257-8972(99)00342-4.

[6]   H.I. Faraoun, T. Grosdidier, J.-L. Seichepine, D. Goran, H. Aourag, C. Coddet, J.
        Zwick, N. Hopkins, Improvement of thermally sprayed abradable coating by
        microstructure control, Surf. Coatings Technol. 201 (2006) 2303–2312.
        doi:10.1016/j.surfcoat.2006.03.047.

[7]   M.S. Mahdipoor, F. Tarasi, C. Moreau, A. Dolatabadi, M. Medraj, HVOF sprayed
        coatings of nano-agglomerated tungsten-carbide/cobalt powders for water droplet
        erosion application, Wear. 330–331 (2015) 338–347. doi:10.1016/j.wear.2015.02.034.

[8]   D. Toma, W. Brandl, G. Marginean, Wear and corrosion behaviour of thermally
        sprayed cermet coatings, Surf. Coatings Technol. 138 (2001) 149–158.
        doi:10.1016/S0257-8972(00)01141-5.

[9]   M. Mohanty, R.W. Smith, M. De Bonte, J.P. Celis, E. Lugscheider, Sliding wear
        behavior of thermally sprayed 75/25 Cr3C2/NiCr wear resistant coatings, Wear. 198
        (1996) 251–266. doi:10.1016/0043-1648(96)06983-9.

[10]   N. Sharifi, F. Ben Ettouil, M. Mousavi, M. Pugh, C. Moreau, A. Dolatabadi,
        Superhydrophoibcity and Water Repelling Characteristics of Thermally Sprayed

Coatings, in: Int. Therm. Spray Conf. Expo., Asm, 2013.

[11] N. Sharifi, M. Pugh, C. Moreau, A. Dolatabadi, Developing hydrophobic and superhydrophobic TiO2 coatings by plasma spraying, Surf. Coatings Technol. (2016). doi:10.1016/j.surfcoat.2016.01.029.

[12] M. Aghasibeig, A. Dolatabadi, R. Wuthrich, C. Moreau, Three-dimensional electrode coatings for hydrogen production manufactured by combined atmospheric and suspension plasma spray, Surf. Coatings Technol. 291 (2016) 348–355. doi:10.1016/j.surfcoat.2016.02.065.

[13] M. Aghasibeig, C. Moreau, A. Dolatabadi, R. Wuthrich, Fabrication of nickel electrode coatings by combination of atmospheric and suspension plasma spray processes, Surf. Coatings Technol. 285 (2016) 68–76. doi:10.1016/j.surfcoat.2015.11.025.

[14] H. Yoon, H. Kim, S.S. Latthe, M. Kim, S. Al-Deyab, S.S. Yoon, A highly transparent self-cleaning superhydrophobic surface by organosilane-coated alumina particles deposited via electrospraying, J. Mater. Chem. A. 3 (2015) 11403–11410. doi:10.1039/C5TA02226F.

[15] C. Peng, S. Xing, Z. Yuan, J. Xiao, C. Wang, J. Zeng, Preparation and anti-icing of superhydrophobic PVDF coating on a wind turbine blade, Appl. Surf. Sci. 259 (2012) 764–768. doi:10.1016/j.apsusc.2012.07.118.

[16] J. Durret, N. Frolet, C. Gourgon, Hydrophobicity and anti-icing performances of nanoimprinted and roughened fluoropolymers films under overcooled temperature, Microelectron. Eng. 155 (2016) 1–6. doi:10.1016/j.mee.2016.01.011.

[17] G. Azimi, H.-M. Kwon, K.K. Varanasi, Superhydrophobic surfaces by laser ablation of rare-earth oxide ceramics, MRS Commun. 4 (2014) 1–5. doi:10.1557/mrc.2014.20.

[18] C.-H. Xue, S.-T. Jia, H.-Z. Chen, M. Wang, Superhydrophobic cotton fabrics prepared by sol–gel coating of TiO2 and surface hydrophobization, Sci. Technol. Adv. Mater. 9 (2008) 35001–5. doi:10.1088/1468-6996/9/3/035001.

[19] X. Zhang, M. Järn, J. Peltonen, V. Pore, T. Vuorinen, E. Levänen, T. Mäntylä, Analysis of roughness parameters to specify superhydrophobic antireflective boehmite films made by the sol-gel process, J. Eur. Ceram. Soc. 28 (2008) 2177–2181. doi:10.1016/j.jeurceramsoc.2008.02.020.

[20] P. Fauchais, M. Vardelle, A. Vardelle, L. Bianchi, Plasma spray: Study of the coating generation, Ceram. Int. 22 (1996) 295–303. doi:10.1016/0272-8842(95)00106-9.

[21] P. Fauchais, M. Fukumoto, a. Vardelle, M. Vardelle, Knowledge Concerning Splat Formation: An Invited Review, J. Therm. Spray Technol. 13 (2004) 337–360. doi:10.1361/10599630419670.

[22] C. Moreau, P. Gougeon, M. Lamontagne, V. Lacasse, G. Vaudreuil, P. Cielo, On-line control of the plasma spraying process by monitoring the temperature, velocity, and trajectory of in-flight particles, ASM International, Materials Park, OH (United States), 1994.

[23] C. Moreau, Towards a better control of thermal spray processes, National Research Council Canada, Industrial Materials Institute, 1997.

[24] G. Mauer, R. Vaßen, D. Stöver, Comparison and applications of DPV-2000 and accuraspray-g3 diagnostic systems, J. Therm. Spray Technol. 16 (2007) 414–424. doi:10.1007/s11666-007-9047-2.

[25] Z. Li, Y. Zheng, J. Zhao, L. Cui, Wettability of atmospheric plasma sprayed Fe, Ni, Cr and their mixture coatings, J. Therm. Spray Technol. 21 (2012) 255–262. doi:10.1007/s11666-011-9728-8.

[26] Z. Li, Y. Zheng, L. Cui, Preparation of metallic coatings with reversibly switchable wettability based on plasma spraying technology, J. Coatings Technol. Res. 9 (2012) 579–587. doi:10.1007/s11998-011-9390-6.

[27] C.-J. Li, Preparation and Characterization of Super-Hydrophobic Surface Through Particle Deposition by Vacuum Cold Spray, in: Int. Therm. Spray Conf. Expo., Asm,

2012.

[28] R. a. Bidkar, L. Leblanc, A.J. Kulkarni, V. Bahadur, S.L. Ceccio, M. Perlin, Skin-friction drag reduction in the turbulent regime using random-textured hydrophobic surfaces, Phys. Fluids. 26 (2014) 85108. doi:10.1063/1.4892902.

[29] L.S. Leblanc, J.A. Ruud, K.P. Mcevoy, A.J. Kulkarni, Methods of coating a surface and articles with coated surface, 2014. http://www.google.com/patents/US20140178641.

[30] X. Chen, Y. Gong, D. Li, H. Li, Robust and easy-repairable superhydrophobic surfaces with multiple length-scale topography constructed by thermal spray route, Colloids Surfaces A Physicochem. Eng. Asp. 492 (2016) 19–25. doi:10.1016/j.colsurfa.2015.12.017.

[31] K. VanEvery, M.J.M. Krane, R.W. Trice, Parametric study of suspension plasma spray processing parameters on coating microstructures manufactured from nanoscale yttria-stabilized zirconia, Surf. Coatings Technol. 206 (2012) 2464–2473. doi:10.1016/j.surfcoat.2011.10.051.

[32] R. Jaworski, L. Pawlowski, F. Roudet, S. Kozerski, A. Le Maguer, Influence of suspension plasma spraying process parameters on TiO 2 coatings microstructure, J. Therm. Spray Technol. 17 (2008) 73–81. doi:10.1007/s11666-007-9147-z.

[33] E. Moreau, C. Chazelas, G. Mariaux, a. Vardelle, Modeling the Restrike Mode Operation of a DC Plasma Spray Torch, J. Therm. Spray Technol. 15 (2006) 524–530. doi:10.1361/105996306X147306.

[34] M.M. Gentleman, J.A. Ruud, Role of Hydroxyls in Oxide Wettability, Langmuir. 26 (2010) 1408–1411. doi:10.1021/la903029c.

[35] A.F. Stalder, G. Kulik, D. Sage, L. Barbieri, P. Hoffmann, A snake-based approach to accurate determination of both contact points and contact angles, Colloids Surfaces A Physicochem. Eng. Asp. 286 (2006) 92–103. doi:10.1016/j.colsurfa.2006.03.008.

[36] A.F. Stalder, T. Melchior, M. Müller, D. Sage, T. Blu, M. Unser, Low-bond axisymmetric drop shape analysis for surface tension and contact angle measurements of sessile drops, Colloids Surfaces A Physicochem. Eng. Asp. 364 (2010) 72–81. doi:10.1016/j.colsurfa.2010.04.040.

[37] M. Miwa, A. Nakajima, A. Fujishima, K. Hashimoto, T. Watanabe, Effects of the Surface Roughness on Sliding Angles of Water Droplets on Superhydrophobic Surfaces, Langmuir. 16 (2000) 5754–5760. doi:10.1021/la991660o.

[38] C. Yang, U. Tartaglino, B.N.J. Persson, Influence of Surface Roughness on Superhydrophobicity, Phys. Rev. Lett. 97 (2006) 116103. http://link.aps.org/doi/10.1103/PhysRevLett.97.116103.

[39] J.I. Rosales-Leal, M.A. Rodríguez-Valverde, G. Mazzaglia, P.J. Ramón-Torregrosa, L. Díaz-Rodríguez, O. García-Martínez, M. Vallecillo-Capilla, C. Ruiz, M.A. Cabrerizo-Vílchez, Effect of roughness, wettability and morphology of engineered titanium surfaces on osteoblast-like cell adhesion, Colloids Surfaces A Physicochem. Eng. Asp. 365 (2010) 222–229. doi:10.1016/j.colsurfa.2009.12.017.

[40] B. Bhushan, Y.C. Jung, Natural and biomimetic artificial surfaces for superhydrophobicity, self-cleaning, low adhesion, and drag reduction, Prog. Mater. Sci. 56 (2011) 1–108. doi:10.1016/j.pmatsci.2010.04.003.

[41] K. Vanevery, M.J.M. Krane, R.W. Trice, H. Wang, W. Porter, M. Besser, D. Sordelet, J. Ilavsky, J. Almer, Column formation in suspension plasma-sprayed coatings and resultant thermal properties, J. Therm. Spray Technol. 20 (2011) 817–828. doi:10.1007/s11666-011-9632-2.

[42] P. Sokolowski, L. Pawlowski, D. Dietrich, T. Lampke, D. Jech, Advanced Microscopic Study of Suspension Plasma-Sprayed Zirconia Coatings with Different Microstructures, J. Therm. Spray Technol. 25 (2016) 94–104. doi:10.1007/s11666-015-0310-7.

[43]   F.-L. Toma, G. Bertrand, D. Klein, C. Coddet, C. Meunier, Nanostructured
photocatalytic titania coatings formed by suspension plasma spraying, J. Therm. Spray
Technol. 15 (2006) 587–592.

[44]   Z. Guo, W. Liu, B.L. Su, Superhydrophobic surfaces: From natural to biomimetic to
functional, J. Colloid Interface Sci. 353 (2011) 335–355.
doi:10.1016/j.jcis.2010.08.047.

Highlights

- Parametric study of suspension plasma sprayed (SPS) titanium dioxide coatings

- Influence of process parameters on morphology and wetting properties of coatings

- Correlation of surface roughness parameters with water mobility and superhydrophobicity

- Insight on developing microtextured coatings with improved superhydrophobicity using

  SPS technique

Highlights